Review



# Research Progress on the Structural Design and Optimization of Silicon Anodes for Lithium-Ion Batteries: A Mini-Review

Zhi Yu , Lijiang Cui , Bo Zhong , Guoxing Qu *

Posted Date: 5 July 2023

doi: 10.20944/preprints202307.0292.v1

Keywords: lithium-ion batteries; silicon anode; structural optimization; surface structural; artificial SEI

*Review*

# Research Progress on the Structural Design and Optimization of Silicon Anodes for Lithium-Ion Batteries: A Mini-Review

**Zhi Yu [1], Lijiang Cui [1], Bo Zhong [1] and Guoxing Qu [1,2,*]**

[1] School of Physics and Materials Science, Nanchang University, Nanchang 330031, Jiangxi, China
[2] Key Laboratory of Advanced Energy Materials Chemistry (Ministry of Education), Nankai University, Tianjin 300071, China
* Correspondence: guoxing.qu@ncu.edu.cn

**Abstract:** Silicon anodes have been considered one of the most promising anode candidates for the next generation of high-energy density lithium-ion batteries due to the high theoretical specific capacity (4200 mAh $g^{-1}$) of Si. However, high lithiation capacity endows silicon anodes with severe volume expansion effects during the charge/discharge cycling. The repeated volume expansions not only lead to the pulverization of silicon particles and the separation of electrode materials from the current collector, but also brings rupture/formation of solid electrolyte interface (SEI) and also continuous electrolyte consumption, which seriously hinders the commercial application of silicon anodes. Structural design and optimization is the key to improving the electrochemical performances of silicon anodes, which has attracted wide attention and research in recent years. This paper mainly summarizes and compares the latest research progress for the structural design and optimization of silicon anodes.

**Keywords:** lithium-ion batteries; silicon anode; structural optimization; surface structural; artificial SEI

## 1. Introduction

With information and communication technology upgrading rapidly, digital products are developing in an increasingly convenient direction, and the demand for the performance of energy storage devices is increasing. Lithium-ion batteries occupy a wide electronics market due to their advantages of high energy density, high output voltage, low self-discharge, no memory effect, long cycle life, and environmental friendliness [1–3]. Nevertheless, with the popularization and rapid development of energy-intensive mobile electronics, such as electric vehicles, smartphones, and drones, the energy density of traditional lithium-ion batteries is no longer meeting the requirement for long endurance [4].

The specific capacity of electrode materials is a crucial factor in determining the energy density of batteries. Currently, the commercial anode for lithium-ion batteries is generally graphite with a theoretical specific capacity of 372 mAh $g^{-1}$. The practical specific capacity of graphite anode in the market has been pushed to 365 mAh $g^{-1}$, approaching its theoretical limit [5], while people's requirements for the energy density of lithium-ion batteries are continuously increasing. It is imperative to develop new anode materials with higher specific capacities. As an environmentally friendly material, Si has an ultrahigh theoretical specific capacity of 4200 mAh $g^{-1}$, which is ten times that of graphite. With the addition of the advantage of high earth abundance, Si has been regarded as one of the most promising anode materials for next-generation lithium-ion batteries [6].

However, the commercial application of silicon anodes is still hindered by its serious volume expansion. The repeated huge volume changes during cycling not only give rise to the pulverization of silicon particles and the separation of electrode materials from the current collector, but also lead to the rupture of the surface SEI, which results in continuous electrolyte consumption and thickening

Preprints (www.preprints.org) | NOT PEER-REVIEWED | Posted: 5 July 2023 doi:10.20944/preprints202307.0292.v1



of the SEI film. Significant efforts have been made to overcome these shortcomings, and various structural design and optimization strategies have been put forward. This paper systematically analyzes the critical problems existing in silicon anodes and summarizes the latest research progress on the structural design and optimization of silicon anodes. The future development direction of silicon anodes is also prospected.

## 2. Problems with silicon anodes

Although silicon anode has many advantages, its commercialization process is still trapped by some problems, mainly in the following three aspects (Figure 1).

Firstly, silicon particles contract and expand in the process of the cycle, and the volume expansion rate can reach 300%, which is the most critical problem in silicon anodes [7]. The huge volume shrinkage and expansion cause silicon anodes to pulverize or rupture and active silicon particles to detach from current collectors, breaking away from electrical contact [8,9]. Second, during the charging and discharging of the first cycle of silicon anodes, a solid electrolyte film will be formed between the electrode surface and electrolyte, also known as SEI. Due to the formation of SEI, a part of the lithium ions from positive electrodes is consumed, and this consumption is irreversible, resulting in lower Coulombic efficiency and specific capacity in the first cycle. The expansion effect of silicon anodes in the cycle process also leads to rupture and regeneration of SEI, which seriously affects cycling performance [10]. All these consequences caused by volume expansion result in a severe capacity fade. Third, silicon is a semiconductor material with poor conductivity ($1\times10^{-3}$ S cm$^{-1}$). As electrode materials, poor conductivity affects the transport of electrons, making the rate performance of lithium-ion batteries poor [11,12].

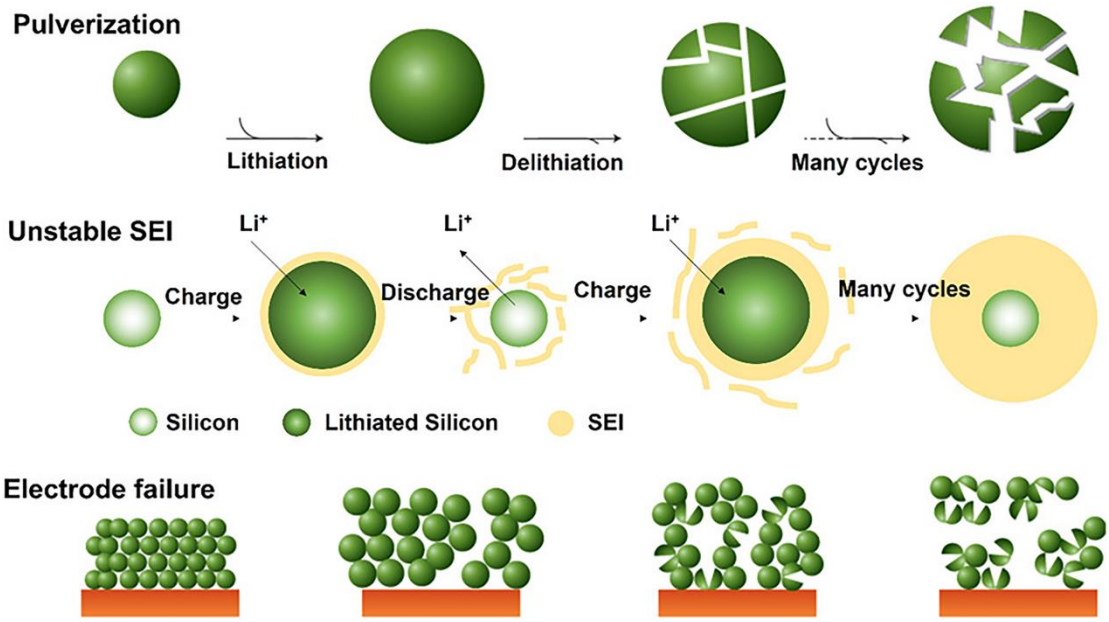


**Figure 1.** The schematic failure modes of silicon anodes during repeated lithiation/delithiation process, including the pulverization and cracking of active Si particles, solid-electrolyte interphase (SEI) formation on the surfaces of Si, and fracture of electrodes. Reproduced with permission [13]. Copyright 2016, Nature Energy.

The above are the main problems of silicon anodes in lithium-ion batteries, and finding efficient solutions is still a challenge.

## 3. Silicon anode structure optimization

To cope with the expansion effect of silicon particles, many researches optimize the structure of silicon anodes by changing the source of electrode materials and electrode design. The common

 doi:10.20944/preprints202307.0292.v1



methods to optimize the structure of silicon anodes mainly include reducing the size of silicon particles, preparing porous silicon and designing silicon anodes without a current collector or binder.

*3.1. Size reduction*

Most commercial Si materials use micron-sized because the cost of micron-sized particles is low. But micron-sized Si has serious volume expansion during the cycle process, resulting in particle pulverization or rupture. Reducing the particle size of Si particles can release stress in the material. At the same time, the surface contact area with the electrolyte is increased, the electron migration distance is shortened, and the conductivity rate is increased [14]. Many studies (reported by Demirkan [15], Lee [16], Chen [17], Park [18], Nogroho [19] and Zhao [20] et al.) have prepared nanoscale Si materials with different shapes or structures, all of which exhibit excellent electrochemical performances.

Bang et al. [21] prepared uniformly sized porous silicon nanowire anodes by block copolymer lithography. Chan's group [22] used gold as a catalyst to grow silicon whiskers vertically on stainless steel foil by VLS (gas-liquid-solid growth) method to prepare a high-performance silicon nanowire anode (Figure 2A). The initial discharge specific capacity of the silicon nanowire anode reached the maximum theoretical value of 4200 mAh $g^{-1}$ and the discharge specific capacity maintained as high as 3500 mAh $g^{-1}$ after 20 cycles at 0.2 C. At a high rate of 1 C, there was still a discharge specific capacity of 2100 mAh $g^{-1}$. The diameter of the silicon nanowires before cycling was about 89 nm and mildly grew to 141 nm after cycling. There was no distinct rupture during cycling.

Tamirat et al. [23] prepared ultra-thin silicon nanolayers for the implantation of $Ni_xSi$/Ni nanoparticles. Sakabe et al. [24] successfully obtained porous amorphous silicon film anodes. Wang et al. [25] synthesized multilayer silicon films by radio frequency magnetron sputtering. Chen et al. [26] prepared a silicon film anode by sputtering silicon on copper foil via a magnetron sputtering method, and retained a reversible capacity of 1300 mAh $g^{-1}$ after 500 cycles at 0.5 C. Compared with the traditional vapor deposition method, this method makes the contact between active materials and the current collector more close and forms a Si-Cu layer, preventing the separation of silicon particles from current collector to a certain extent.

It is still challenging to achieve sub-nanometer (<1 nm) size silicon particles. Sung et al. [27] used ethylene as a growth inhibitor to prevent silicon particles from continuously growing after chemical vapor nucleation, successfully preparing sub-nanometer size silicon particles. Sub-nanometer size silicon anodes enhance cycle stability, with a coulomb efficiency of 98.5% after 99 cycles. In a 110 Ah full battery, a high capacity retention of 91% after 2875 cycles was obtained. The small particle size increases the specific surface area of active materials, reduces the stress of volume expansion, resists to pulverize, increases the contact area with electrolyte, shortens the ion migration distance, and improves the charge and discharge efficiency.

Karuppiah et al. [28] used a simple and scalable method to grow silicon nanowires on graphite to obtain Gt-SiNM composite materials, with using diphenyl silane as silicon source and gold as a catalyst (Figure 2B). The uniform distribution of SiNM and graphite flakes prevents electrode pulverization and alleviates the volume expansion of Si. The capacity retention rate reached 87% after 250 cycles at 2 C rate.

Compared with solid nanowire structure, hollow nanotube structure has more advantages in resisting volume expansion. Wen et al. [29] prepared silicon nanotubes by magnesium thermal reduction, which showed much improved electrochemical performances. Park et al. [30] used alumina as a template to restore decomposition of the silicon precursor, and then etched Si nanotubes, finally depositing a carbon coating on the surface of Si nanotubes (Figure 2C). The initial outer diameter of Si nanotubes is 200-250 nm, and the wall thickness is 40 nm. During the cycle process, Si nanotubes act as pathways for lithium ions and increase the ion migration rate. At 1 C rate, the Si nanotubes had a reversible specific capacity of 3247 mAh $g^{-1}$ and a capacity retention rate of 89% after 200 cycles. The thickness of Si nanotubes increased to 300 nm after 200 cycles, but the Si nanotubes were not crushed.

Preprints (www.preprints.org) | NOT PEER-REVIEWED | Posted: 5 July 2023 doi:10.20944/preprints202307.0292.v1



Many studies have shown that hollow structures combining nanominiaturization are more effective to mitigate volume expansion of Si. For instances, Ashuri et al. [31] obtained carbon-coated hollow silicon nanospheres, which showed better cycle stability than micron size. Liang et al. [32] designed silica sol into porous silicon nanospheres by hydrothermal method. Pu et al. [33] prepared silicon nanospheres by a simple and expandable spray drying method, and used fulvic acid (FA) as a carbon source to prepare carbon shells coated on the silicon spheres (Figure 2D). There is some space between the carbon shells and the silicon spheres to buffer volume expansion. Fulvic acid has wealthy functional groups that bond with silicon particles to form secondary particles. Due to the nanosphere structure of silicon carbon composite electrodes Si@FA, they have significantly better electrochemical performance than pure silicon electrodes. After 100 cycles at a current density of 0.1 A $g^{-1}$, it had a reversible specific capacity of 917.28 mAh $g^{-1}$.

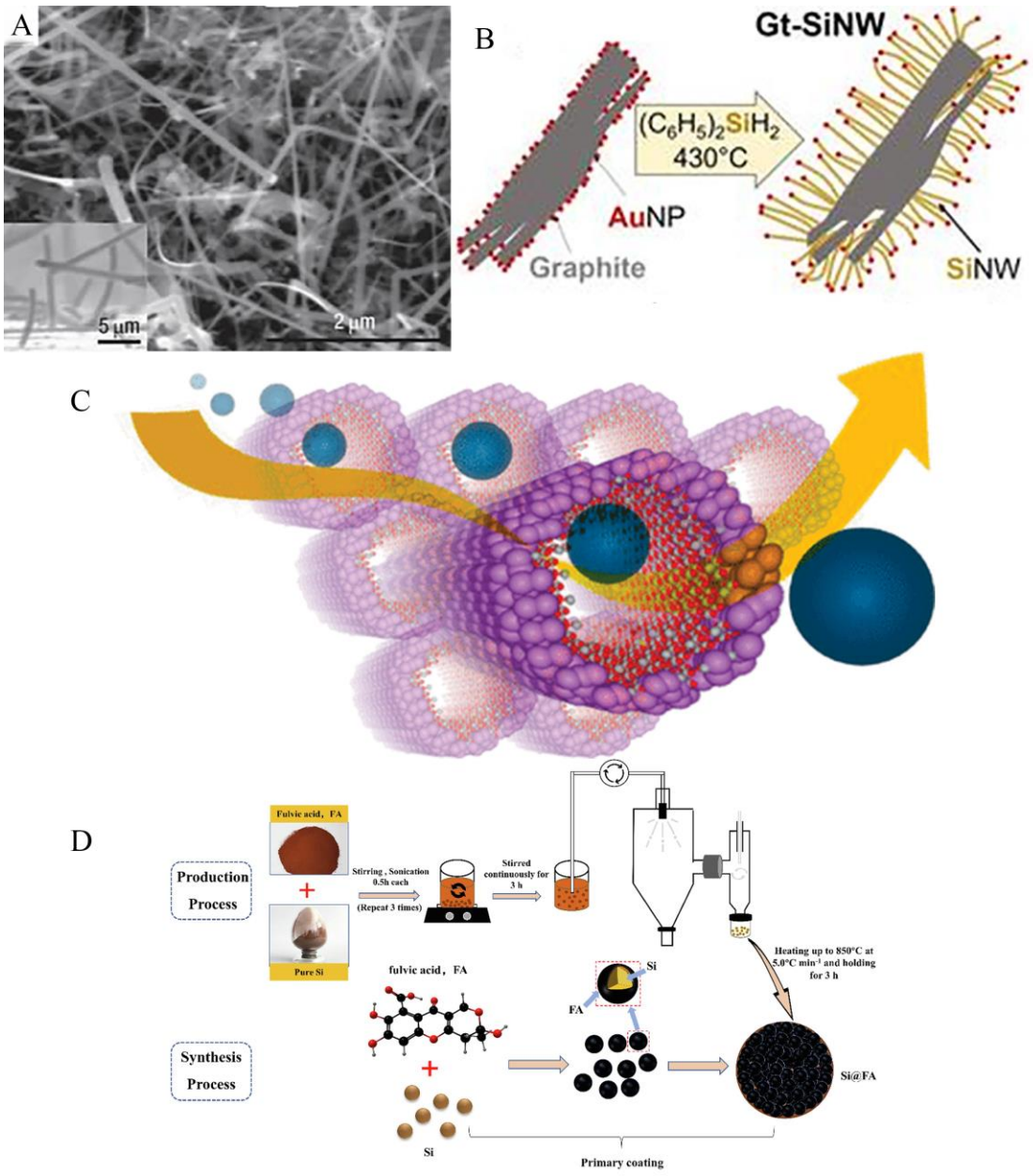


**Figure 2.** A. SEM image of silicon nanowires. Reproduced with permission [22]. Copyright 2008, Nature Nanotechnology. B. Scheme represents the synthesis of SiNWs on graphite. Reproduced with permission [28]. Copyright 2020, ACS Nano. C. Schematic diagram of Li-ion pathway in Si nanotubes. Reproduced with permission [30]. Copyright 2009, Nano Letters. D. Schematic of the preparation procedure of Si@FA-X. Reproduced with permission [33]. Copyright 2022, Chemical Physics Letters.

Preprints (www.preprints.org) | NOT PEER-REVIEWED | Posted: 5 July 2023 doi:10.20944/preprints202307.0292.v1



*3.2. Porous structure*

In addition to reducing the dimensions of silicon particles, creating space for the expansion of silicon particles can also somewhat buffer the volume expansion. Create space by porous particles in the silicon itself. During the cycle, the expansion will preferentially grow towards the pores. To some extent, it inhibits the volume expansion of the overall electrode, effectively prevents electrode pulverization or rupture, and improves the electrochemical performance of the battery.

Tesfaye et al. [34] prepared porous Si nanotubes on stainless steel substrates by sacrificing the ZnO nanowire template method. Saager et al. [35] deposited silicon and zinc under a vacuum, then annealed to remove the zinc, resulting in a porous silicon film (Figure 3A). The Zn in the film can be almost removed (Figure 3B), leaving a pore size of approximately nanometers to micrometers. Compared with dense silicon thin films, the electrochemical performance has improved, but the cyclic stability is insufficient for practical applications. The electrode with a Si loading mass of 0.56 mg $cm^{-2}$ showed a reversible specific capacity of 1300 mAh $g^{-1}$ after 30 cycles at a rate of 0.1 C. When the loading mass of Si is 0.46 mg $cm^{-2}$, the capacity can remain stable for over 150 cycles.

Jin et al. [36] easily synthesized porous silicon structures by magnesium thermal reduction and $TiSi_2$-coated. Li et al. [37] used electrochemical etching to produce a large mesoporous silicon sponge (MSS) with a pore diameter of approximately 50 nm (Figure 3C). This structure accommodates most volume changes and limits the volume expansion to 30%. Compared to the 300% volume expansion of traditional silicon electrodes, it greatly reduces the volume expansion effect and does not cause electrode pulverization even after 1000 cycles. After 1000 cycles at a current density of 1 A $g^{-1}$, this unique structure still had a capacity of 750 mAh $g^{-1}$ based on the entire electrode mass, with a capacity retention rate of 80%.

Yan et al. [38] designed porous silicon nanoparticles by a simple alkaline etching method, which can adapt to the large volume expansion of silicon. Ge et al. [39] synthesized porous doped silicon nanowires by direct etching boron-doped silicon wafers. There are also studies on preparing silicon into a spherical, hollow, and porous structure. Xiao et al. [40] synthesized $SiO_2$ by condensation and hydrolysis of tetraethoxysilane and octadecyl trimethoxysilane, then converted $SiO_2$ into Si by Mg steam (Figure 3D), and finally removing MgO through acidification to prepare porous hollow silicon spheres (hp-SiNSs). The unique structure converts the volume expansion inward, and the electrode will not be powdered, improving the electrochemical performance. Under 0.05 C rate, the capacity was 1800 mAh $g^{-1}$ after 200 cycles.

An et al. [41] prepared an ant nest-like block porous silicon anode. Mg was alloyed with Si powder to generate $Mg_2Si$, and the byproduct $Mg_3N_2$ was removed through $N_2$ nitridation followed by acidification to separate ant nest-like porous silicon (AMPSi). Finally, a carbon coating was applied to prepare AMPSi@C (Figure 3E). The porous silicon anode of three-dimensional interconnected nanoribbons and continuous nanopores prevents electrode pulverization and volume expansion during cycling. The AMPSi@C released a capacity of 1271 mAh $g^{-1}$ after 1000 cycles at 2100 mA $g^{-1}$, with a capacity retention rate of 90%. At a high area capacity of 5.1 mAh $cm^{-2}$, the expansion rate was only 17.8%.

Similar porous composite silicon anodes have been widely reported. Dong et al. [42] synthesized Si@C porous composites in situ to achieve low expansion rates. Hu et al. [43] prepared silicon/carbon composite porous nano-anodes to achieve high cycle stability. Jia et al. [44] obtained CNT@Si yarn-like spheres by in-situ aluminothermic reduction of CNT@$SiO_2$ core-shell tubular microspheres, and coated the spheres with a carbon layer, ultimately obtaining CNT@Si@C microspheres (Figure 3F). The Si in CNT@Si@C was obtained by the reduction of $SiO_2$, bring a porous structure. The volume expansion of CNT@Si after lithiation was only 1/10 of the original volume, CNT@Si@C had 40% volume expansion. At a current density of 1 mA $cm^{-1}$, the reversible specific capacity of the electrode was about 1500 mAh $g^{-1}$, and the capacity retention rate was 87% after 1500 cycles.

Preprints (www.preprints.org) | NOT PEER-REVIEWED | Posted: 5 July 2023 doi:10.20944/preprints202307.0292.v1



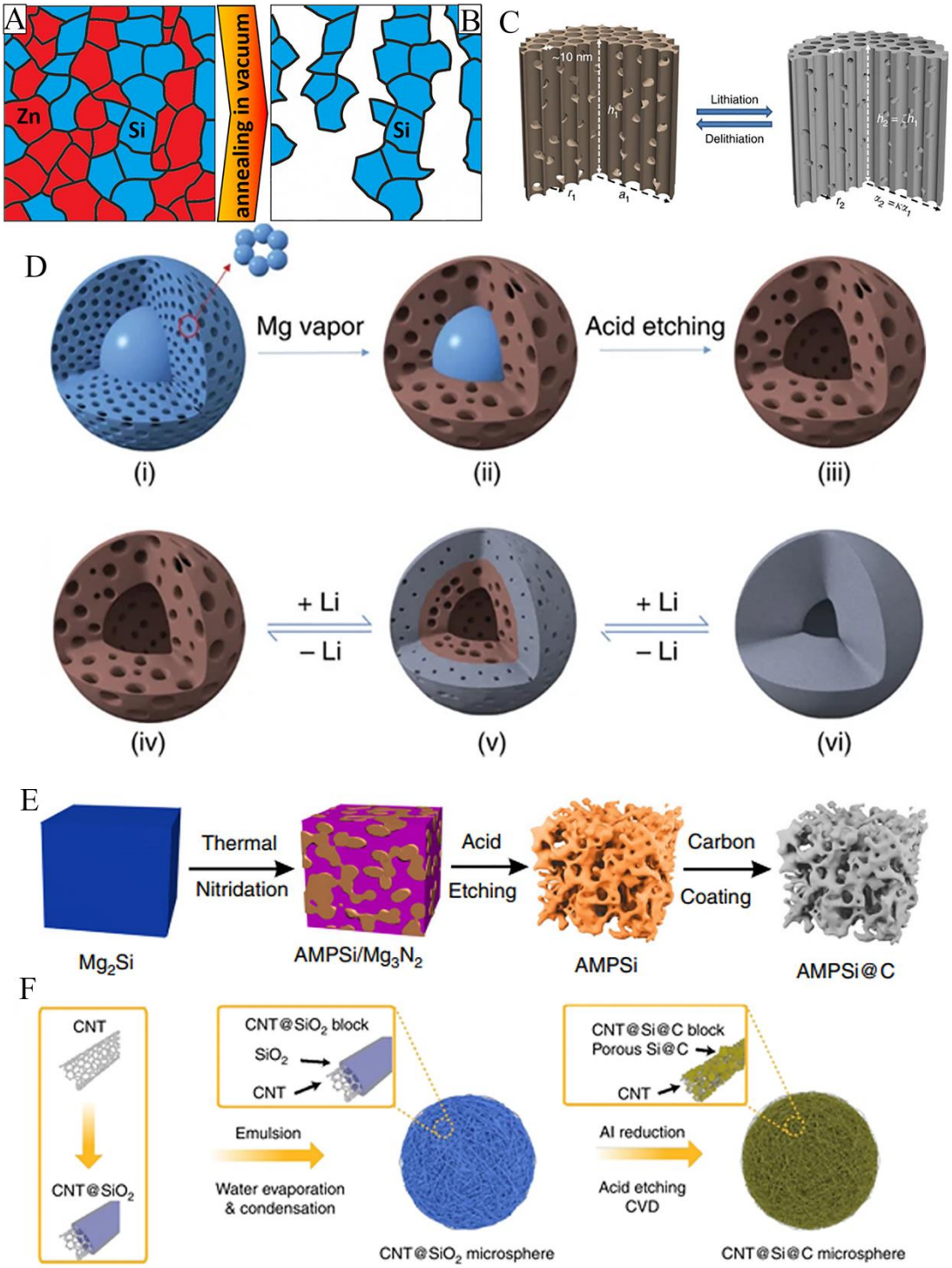


**Figure 3.** A. Scheme of forming separated grains of zinc (red) and silicon (blue) after deposition. B. Scheme of porous silicon film after expelling zinc by thermal annealing. Reproduced with permission.[35] Copyright 2019, Surface and Coatings Technology. C. A schematic model of the MSS particle. Reproduced with permission.[37] Copyright 2014, Nat Commun. D. Schematic diagram of the synthesis of hp SiNS and the lithiation/delithiation process of hp SiNSs shows that the mesoporous shell expands its volume towards the internal hollow during the lithiation process and restores its morphology during the delithiation process. Reproduced with permission.[40] Copyright 2015, Nat Commun. E. Schematic diagram of preparation process of AMPSi and AMPSi@C. Reproduced with permission.[41] Copyright 2019, Nat Commun. F. Schematic figure showing the synthesis of CNT@Si@C microspheres. Reproduced with permission.[44] Copyright 2020, Nat Commun.

Preprints (www.preprints.org) | NOT PEER-REVIEWED | Posted: 5 July 2023 doi:10.20944/preprints202307.0292.v1



*3.3. Free binder or current collector of silicon anode*

During the cycle process, the expansion and pulverization of silicon particles leads to the detachment of active substances from collector, silicon particles loss of electrical contact, and thus severe capacity fading. The traditional preparation method involves mixing active substances, conductive carbon black, and binders in a ratio of 8:1:1 and coating them on copper foil. Some existing studies have prepared silicon anode without binders or current collectors. Compared with traditional electrode preparation methods, the advantage is preventing active substances from peeling off the current collector during the shrinkage and expansion process, reducing the electrode load and saving costs.

Guo et al. [45] synthesized a porous carbon skeleton structure to alleviate the expansion of silicon volume and eliminate the binder. Dong et al. [46] added a small amount of Sn to the slurry to carbonize the original binder into a conductive skeleton. Sn was melted and extruded by hot pressing, and was cooled to bond Si particles. During the process, $Cu_3Si$ and $Cu_3Sn$ interlayers were formed on the surface of the current collector, causing the active substance to bind closely to the current collector. The electrode was hot pressed to half of its original state, but still exhibited excellent electrochemical performance, maintaining a capacity of 932 mAh $g^{-1}$ after 500 cycles at a current density of 1500 mA $g^{-1}$. The rate performance had also been enhanced, with a specific discharge capacity of 1075 and 773 mAh $g^{-1}$ at 3000 and 4500 mA $g^{-1}$ current densities. This electrode type has high conductivity and density, which can achieve high volume capacity.

Favors et al. [47] synthesized nanofiber silicon paper electrodes by $SiO_2$ through magnesium thermal reduction and electrospinning, then used $C_2H_2$ as a carbon source to coat the silicon paper electrodes with carbon (Figure 4A). The independent carbon-coated silicon nanofiber anode has neither binder nor a current collector, reducing the electrode load and increasing the proportion of active substances. On this electrode, the proportion of silicon exceeded 80%. After 659 cycles at a rate of 0.1 C, it displayed a capacity of 802 mAh $g^{-1}$, with a Coulombic efficiency of 99.9%. Compared to graphite electrodes prepared by traditional methods, the capacity is more than twice that.

Zhu et al. [48] connected the three-dimensional interconnected nitrogen/carbon network hollow carbon nanospheres and silicon nanodots, and finally obtained a binder-free SHCM/NCF anode. Zhang et al. [49] encapsulated the silicon particles in multilayer graphene to prepare an RGO/Si anode without a binder. Liu et al. [50] prepared silicon nanowires by CVD method, and uniformly distributed silicon nanowires on carbon cloth through electrospinning to prepare a binder-free silicon anode (Figure 4B). The specific surface area of carbon cloth coated increases, and there are more active sites for lithium-ion. The close contact between silicon and carbon also increases the material's conductivity. After 200 cycles at 0.2 C, the binder-free silicon nanowire anode showed a specific capacity of 2950 mAh $g^{-1}$ and a capacity retention rate of 92%.

Wang et al. [51] prepared a silicon anode by directly arranging silicon/carbon nanotubes vertically on Inconel current collector, avoiding polymer binders. Haro et al. [52] organized a special binder-free silicon anode, which was supported by the vapor deposition of TaNS (Figure 4C). The columnar amorphous silicon film was deposited on the TaNS support to form an arched structure and annealed. When the diameter of columnar silicon continues to grow, the tips come into contact with each other. Then the anode surface is encapsulated, and stable SEI can be formed on the surface. This structure causes its volume to expand towards the inner cavity at 0.5 C, the initial capacity reached 3230 mAh $g^{-1}$, and the capacity retention rate was 88% after 100 cycles (2832 mAh $g^{-1}$).

Wang et al. [53] synthesized a novel self-supporting adhesive-free silicon-based anode with overlapping graphene and reduced graphene oxide wrapped silicon nanowires (SiNW). Li et al. [54] prepared Si/C composites by electrospinning. Si adhered to the outside of the carbon tube, and Si/C was used as the core. Then carbon coated the structure to obtain the final Si/C-C material (Figure 4D). Si/C-C as an independent fiber conductive film without the addition of conductive agents and binders, can be directly used as an electrode. The connection between the silicon and carbon shell cushions the stress generated by the volume expansion of silicon during the cycling process, making the electrode have good cycling stability. At a current density of 50 mA $g^{-1}$, the specific capacity was 886.5 mAh $g^{-1}$, and the capacity retention rate was 72.4% after 50 cycles.

 doi:10.20944/preprints202307.0292.v1



Shao et al. [55] prepared a binder-free anode by wrapping silicon particles in a three-dimensional conductive network of flexible graphene-fiber-fabric (GFF). Liu et al. [56] also designed a hollow structure binder-free Si-Ni-C silicon anode by electrospinning; there was no sacrificial material in this process. The addition of Ni improved the conductivity of the composite material. This composite material maintained a specific capacity of 622 mAh $g^{-1}$ after 100 cycles at a current density of 100 mA $g^{-1}$.

Most binder-free or collector-free electrodes are prepared by electrospinning in combination with other methods. Osaka et al. [57] crafted a binder-free Si-O-C composite film showing excellent cycle durability by electrodeposition. Yang et al. [58] prepared a binder-free silicon anode in an organic solvent by one-step electrophoretic deposition (EPD). Under the action of electrophoretic deposition, nano silicon and acetylene black (AB) form interconnected 3D deposition films (Figure 4E). The close contact between Si and AB shortens the ion migration distance and improves the charge transfer efficiency. The structure of the 3D network provides buffer space for silicon expansion. It was found that the electrode prepared under 5S EPD deposition performs best. Even at a high rate of 1 C and 2 C, the electrode showed a specific capacity of 1516 mAh $g^{-1}$ and 1231 mAh $g^{-1}$ after 200 cycles, respectively.

Preprints (www.preprints.org) | NOT PEER-REVIEWED | Posted: 5 July 2023 doi:10.20944/preprints202307.0292.v1



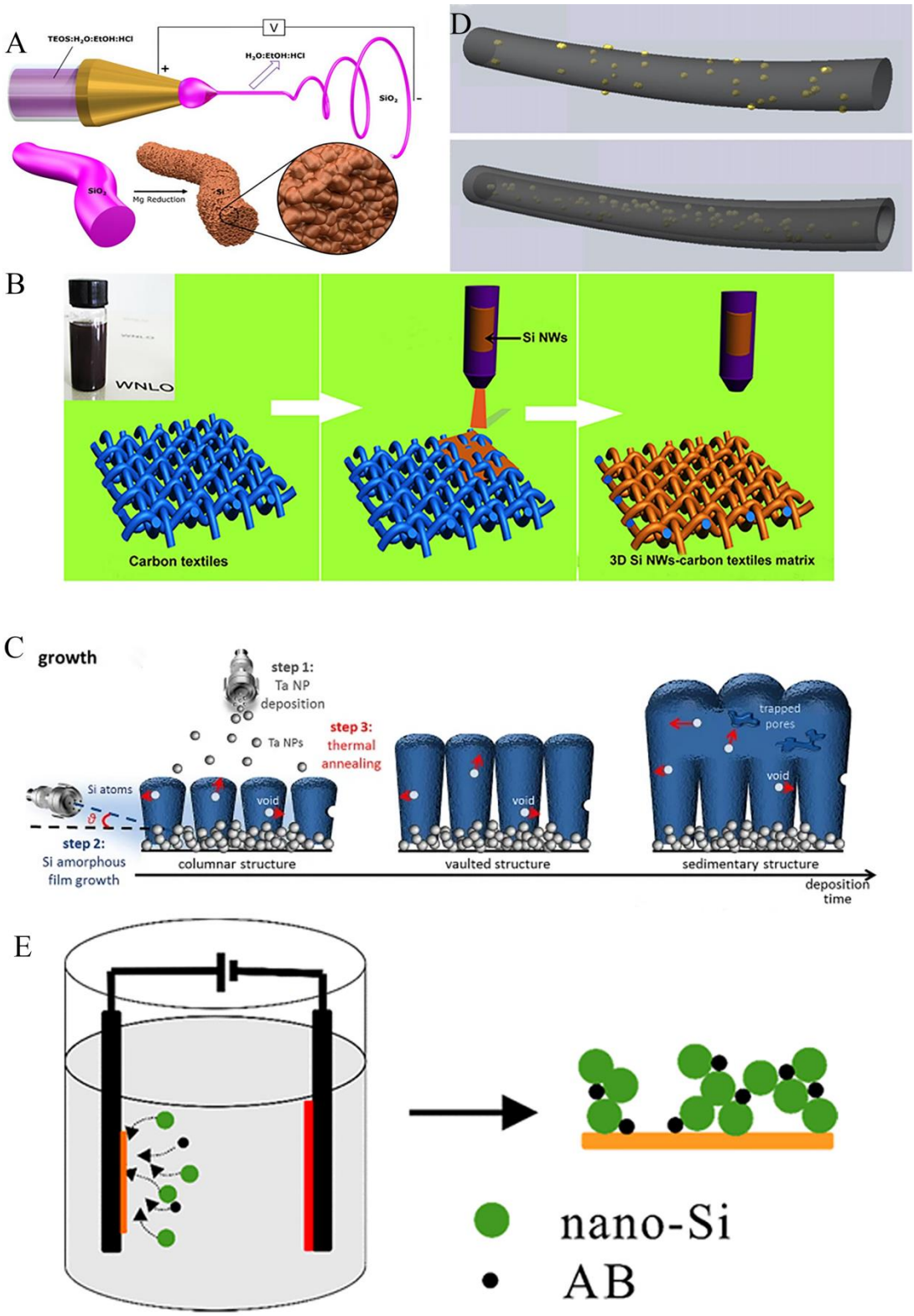


**Figure 4.** A. Schematic diagram of the electrospinning process and subsequent reduction process. Reproduced with permission.[47] Copyright 2015, Scientific Reports. B. Schematic illustration of the formation of hierarchical silicon-carbon textiles matrix. Reproduced with permission.[50] Copyright 2013, Scientific Reports. C. Schematic breakdown of growth process into three steps: deposition of TaNS, columnar growth of silicon amorphous film exploiting the shadowing effect of the TaNS and thermal annealing at 150 °C enhancing the mobility and consequent annihilation of voids at open surfaces. Reproduced with permission.[52] Copyright 2021, Commun Mater. D. Schematic of Si/C composite nanofibers and Si/C–C core–shell composite nanofibers. Reproduced with

 doi:10.20944/preprints202307.0292.v1



permission.[54] Copyright 2014, Solid State Ionics. E. Schematic of the process for fabrication of EPD electrode. Reproduced with permission.[58] Copyright 2015, *ACS Applied Materials & Interfaces*.

## 4. Optimization of surface structure of silicon anode

Reducing the dimension of silicon particles is a strategy for mitigating volume expansion effect from materials source. Structural optimization can also be carried out outside the silicon particles to leave space for the volume expansion of the silicon particles or provide stress to prevent the silicon particles from continuing to expand. The main methods for optimizing the external structure of silicon particles are to prepare shell-cores structures and sandwich structures.

### *4.1. Coating structure*

There are many studies on the shell core structure in the coating structure, generally using silicon as the core or forming a shell in the outer layer, leaving a particular space between the two. During the cycle process, the expansion of silicon occurs in the space between the shell and core. If the degree of expansion is too large, the shell will have a certain degree of stress that hinders the continuous growth of silicon particles. The shell structure limits the degree of silicon expansion, restrains the pulverization of silicon particles, and prevents direct contact between silicon particles and electrolyte.

Coating structures could not only weaken volume expansion effects, but also improve conductivity. Different coating structures have been designed to obtain high performance silicon anodes. Song et al. [59] prepared a controllable spongy porous nanocarbon-coated silicon (sCCSi). Tan et al. [60] used bitumen as a carbon source to prepare a homogeneous carbon-coated silicon anode. Guan et al. [61] prepared a PSi/C electrode composed of Si/C nanobeads by spray drying and pyrolysis treatment (Figure 5A). In the PSi/C electrode, Si/C nanoparticles with egg yolk structure are uniformly dispersed and interconnected to form a porous three-dimensional framework. There is sufficient space in the egg yolk structure Si/C structure and a porous structure between the carbon frameworks. The shell core structure and the porous structure are placed in one system. Both structures have sufficient space to cope with Si shrinkage and expansion, greatly improving the stability of the battery. The connection of carbon frameworks also contributes to the improvement of conductivity. The mass fraction of active substance Si in the PSi/C electrode was only 15.4%, but it releaseed a specific capacity of 1357.43 mAh $g^{-1}$ at a current density of 100 mA $g^{-1}$. After 100 cycles, it still had a reversible capacity of 933.62 mAh $g^{-1}$. Even at ten times the current density (1000 mA $g^{-1}$), a specific discharge capacity of 610.38 mAh $g^{-1}$ remained after 3000 cycles.

Bionics has been providing new ideas for scientific research. Ma et al. [62] found that the heartbeat has a similar mechanism to the contraction and expansion of silicon particles. Lithium ions flow to silicon when silicon particles expand, as if the heart relaxes. When the silicon particles contract, lithium ions flow out of the silicon particles, similar to the heart pumping blood. So they have prepared the silicon particles into independent heart structures (Figure 5B). Using the CVD method, sheet graphene is cross-linked to form a framework, which is uniformly filled with silicon particles to mimic the "heart". Finally, carbon nanofibers are coated on the outer surface of this structure using electrospinning technology to replace the external arteries and veins of the heart, resulting in the "heart" structure of the G/Si@CFs anode. The coating of carbon nanofibers enhances electron transport, improves conductivity, and prevents the pulverization or rupture of silicon particles under the effect of coating, significantly improving the cycling performance and capacity of lithium-ion batteries. At a current density of 100 mA $g^{-1}$, the G/Si@CFs electrode had a specific capacity of 896.8 mAh $g^{-1}$ and a capacity retention rate of 86.5% after 200 cycles.

Most carbon shells are coated on particles by solvent gel or physical vapor deposition method, which is costly and requires high experimental conditions. Li et al. [63] prepared ball-milled silicon@carbon/reduced graphene oxide composites (bmSi@C/rGO) by electrostatic assembly. Because tannic acid can spontaneously polymerize outside the particles, Feng's team [64] mixed the Si particles with mechanically milled Si/G precursors and tannic acid, then carbonized them to coat the particles with a carbon layer, obtained Si@TA and Si@TA-G samples. The addition of tannic acid coating acts as a barrier between Si and the electrolyte, preventing direct contact between the two

 doi:10.20944/preprints202307.0292.v1



and improving conductivity. After 150 cycles at 100 mA $g^{-1}$, the Si@TA showed a specific capacity of 927.4 mAh $g^{-1}$ and a capacity retention rate of 87.1%. Under the same conditions, Si@TA-G had a capacity of 1249.8 mAh $g^{-1}$ and a capacity retention rate of 93.6%.

Chen et al. [65] successfully realized a copper-coated silicon nanowire anode by chemical vapor deposition and magnetron sputtering. Baek et al. [66] synthesized Ag-coated silicon nanowires by an isomorphic redox reaction. Chan et al. [67] synthesized silicon nanowires using the SFLS method mixed them with multi-walled carbon nanotubes, and then carbon coated them through sucrose pyrolysis. The coating layer of sucrose pyrolysis was found to provide good electrical contact for the material. The carbon-coated silicon nanowire material maintains a capacity of 1500 mAh $g^{-1}$ after 30 cycles at 0.2 C.

Wu et al. [68] synthesized silicon nitride-coated silicon anodes by two-step DC sputtering on a copper microcone array (CMA). He et al. [69] coated an ultra-thin alumina layer on a patterned silicon electrode by atomic layer deposition (ALD). Zhang et al. [70] coated the surface of the porous silicon sphere after magnesium thermal reduction with a nitrogenous carbon layer. Kong et al. [71] used PAN as a carbon and nitrogen source to prepare necklace-shaped silicon nanospheres with nitrogen-doped carbon coating (NL-Si@C) through electrospinning and magnesium thermal reduction (Figure 5C). Silicon nanospheres come from etched $SiO_2$. After being converted into Si, there is room left in the carbon shell for volume expansion. The content of $SiO_2$ can control the proportion of silicon in the material. In nitrogen-doped carbon shells, nanospheres are connected by the carbon shell, shortening ions' migration distance and improving the charge transfer efficiency. At the same time, the obstruction of the carbon layer was also conducive to the formation of stable SEI. The sample of NL-Si@C-0.5 exhibited the best performance, with a specific capacity of 710 mAh $g^{-1}$ after 500 cycles at a current density of 200 mA $g^{-1}$.

Song et al. [72] reported on synthesizing micro-sized silicon-carbon (Si-C) composites with primary sub-10 nm silicon particles and secondary microsize aggregates coated with carbon. Li et al. [73] used Ni NP as a template to prepare CNS, and treated Ni NP with HCl etching. Then, Si and $Al_2O_3$ were deposited on the CNS to obtain a hollow CNS/Si/$Al_2O_3$ shell core membrane structure (Figure 5D). The function of $Al_2O_3$ thin film is to reduce the formation of SEI, provide a good electron transfer channel and improve conductivity by the CNS contacts the surface of silicon particles. This hollow structure serves as a framework, allowing the expansion direction of silicon to move inward, providing buffer space for the volume expansion of silicon during the cycling process. Therefore, the electrode performance exhibits a good specific capacity and a capacity retention rate: after 100 cycles at a current density of 1 A $g^{-1}$, the specific capacity was 1560 mAh $g^{-1}$, and the capacity retention rate reached 85%.

In addition to these carbon coatings, researchers also tried to coat silicon particles with hydrogel. Wu et al. [74] used phytic acid as a gelling agent and prepared PAni from aniline monomer. The nitrogen group on Polyaniline was connected with an aniline monomer to form a cross-linked network hydrogel. Then SiNPs were added to mix and coated on copper foil to prepare a hydrogel silicon anode (Figure 5E). The hydrogel can be in-situ polymerized on the surface of silicon particles and has good conductivity. Multiple pores in the cross-linked network allow silicon to expand, resulting in excellent electrochemical performance of the electrodes. At a high current density of 6 A $g^{-1}$, the hydrogel silicon anode showed a specific capacity of about 550 mAh $g^{-1}$ and a capacity retention rate of 90% after 5000 cycles.

Preprints (www.preprints.org) | NOT PEER-REVIEWED | Posted: 5 July 2023 doi:10.20944/preprints202307.0292.v1



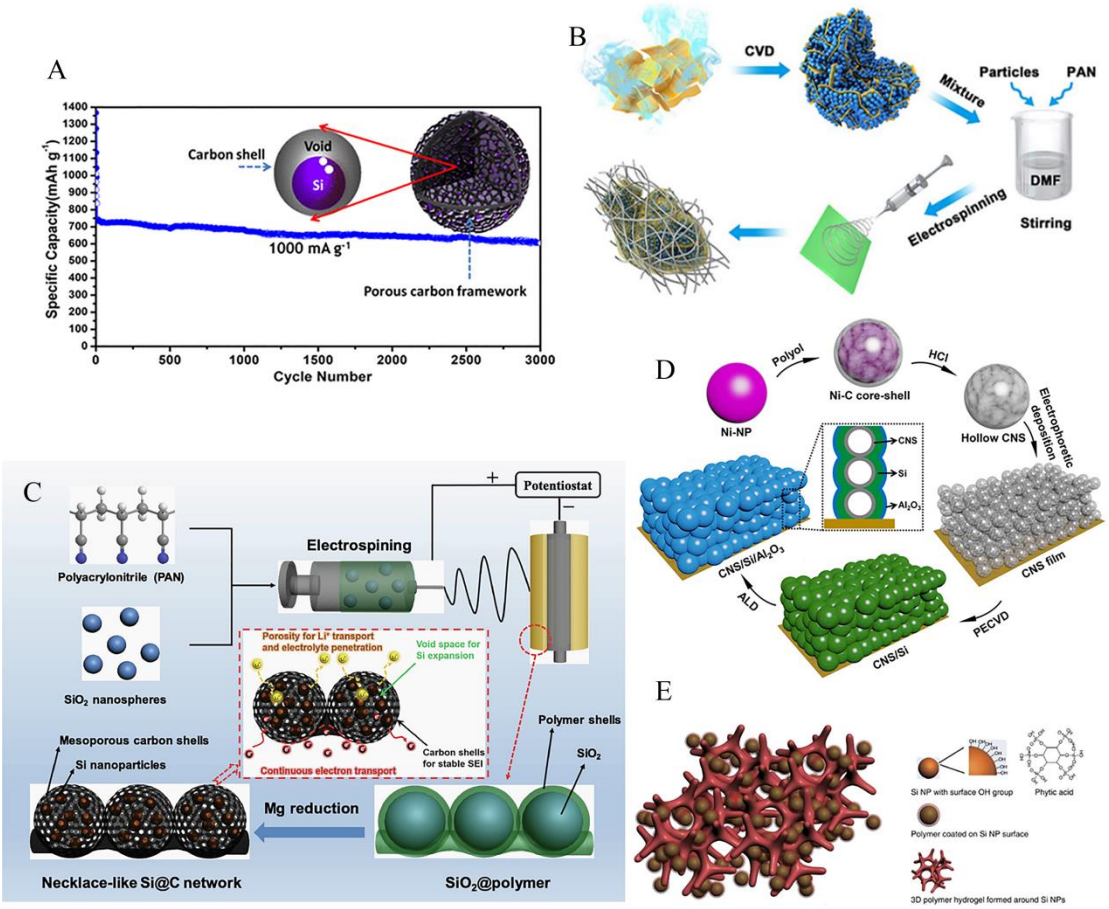


**Figure 5.** A. PSi/C electrode structure and cyclic performance diagram. Reproduced with permission.[61] Copyright 2018, American Chemical Society. B. Biomimetic heart electrode preparation flow chart. Reproduced with permission.[62] Copyright 2017, Scientific Reports. C. Schematic illustration of the synthesis process for a necklace-like Si@C network. Reproduced with permission.[71] Copyright 2019, Science Bulletin. D. Schematic of hollow CNS/Si/$Al_2O_3$ core-shell film fabrication processes. Reproduced with permission.[73] Copyright 2015, Scientific Reports. E. Schematic illustration of 3D porous SiNP/conductive polymer hydrogel composite electrodes. Each SiNP is encapsulated within a conductive polymer surface coating and is further connected to the highly porous hydrogel framework. SiNPs have been conformally coated with a polymer layer either through interactions between surface −OH groups and the phosphonic acids in the crosslinker phytic acid molecules (right column), or the electrostatic interaction between negatively charged −OH groups and positively charged PAni due to phytic acid doping. Reproduced with permission.[74] Copyright 2013, Nat Commun.

### *4.2. Sandwich structure*

The principle of sandwich structure is similar to that of a coating structure. Silicon acts as an intermediate layer of the sandwich structure and does not directly come into contact with the electrolyte. The outer layer of silicon serves as a buffer layer, accommodating the volume expansion of silicon, thereby improving the cycling stability and specific capacity of silicon anodes.

Xu et al. [75] added a carbon layer between the current collector and the active material silicon to prepare a sandwiched silicon anode. The electrochemical performance of pure silicon anode can be optimized using the most traditional and simple method to prepare sandwich structures. Zhao et al. [76] used the most traditional electrode preparation process by coating micrometer-level silicon slurry on copper foil, waiting for drying, and then coating graphene slurry on the silicon layer. The electrode was compacted through a rolling process to prepare a “graphene-silicon-copper” sandwich structure electrode (Figure 6A). It solves the problem of pulverization of silicon particles, ensures

 doi:10.20944/preprints202307.0292.v1



close contact between electrodes, and maintains good electrical contact. Compared to pure silicon and graphene, the initial specific capacity of the sandwich structure was 1700 mAh $g^{-1}$, and its specific capacity decreased to 878 mAh $g^{-1}$ after 30 cycles. After 1200 cycles, it had a reversible capacity of 466 mAh $g^{-1}$, and the performance was the best among the three. This performance advantage comes from the special sandwich structure, which buffers the volume expansion during charging and discharging, and prevents electrode pulverization or rupture, thereby ensuring effective electrical contact.

Zhang et al. [77] prepared sandwiched silicon/$Ti_3C_2T_x$ MXene composites by electrostatic self-assembly. Tian et al. [78] synthesized a flexible and binder-free Si/MXene composite paper anode through valence anchoring and vacuum filtration (Figure 6B). The layered structure design allows silicon nanospheres to be evenly dispersed between interlayers of MXenes. It prevents MXenes from reptile up, promotes lithium ion transport efficiently, and adapts to severe Si volume expansion. Adding MXenes improves the conductivity of electrode, and thus enhances electrochemical performance. At a current density of 200 mA $g^{-1}$, the specific discharge capacity remains at 2118 mAh $g^{-1}$ after 100 cycles. At a current density of 1000 mA $g^{-1}$, it showed a specific discharge capacity of 1672 mAh $g^{-1}$ after 200 cycles. In the rate performance test, the silicon/$Ti_3C_2T_x$ MXene composites offered a reversible capacity of 890 mAh $g^{-1}$ at a high current density of 5000 mA $g^{-1}$.

Sun et al. [79] synthesized a sandwiched graphite-silicon metal@C (MS-G@C) composite, which showed good electrochemical performance. Hassan et al. [80] prepared SG by Hummer method, and added SiNPs, GO, and PAN to mix well and sintered. The layered structure of SG-Si-SG was obtained, and the silicon particles were coated with c-PAN and graphene (Figure 6C). The network structure of graphene and cyclized PAN promote electric charge transfer and improve conductivity. A covalent bond connects Si–S, and the interaction between them also enhances the stability of the long-term cycle. At a current density of 2 A $g^{-1}$, the specific capacity exceeded 1000 mAh $g^{-1}$ after 2275 cycles. At the same time, this layered structure separated the electrolyte and SiNPs, stabilizing the formation of SEI, with Coulombic efficiency of up to 99%.

Preprints (www.preprints.org) | NOT PEER-REVIEWED | Posted: 5 July 2023 doi:10.20944/preprints202307.0292.v1



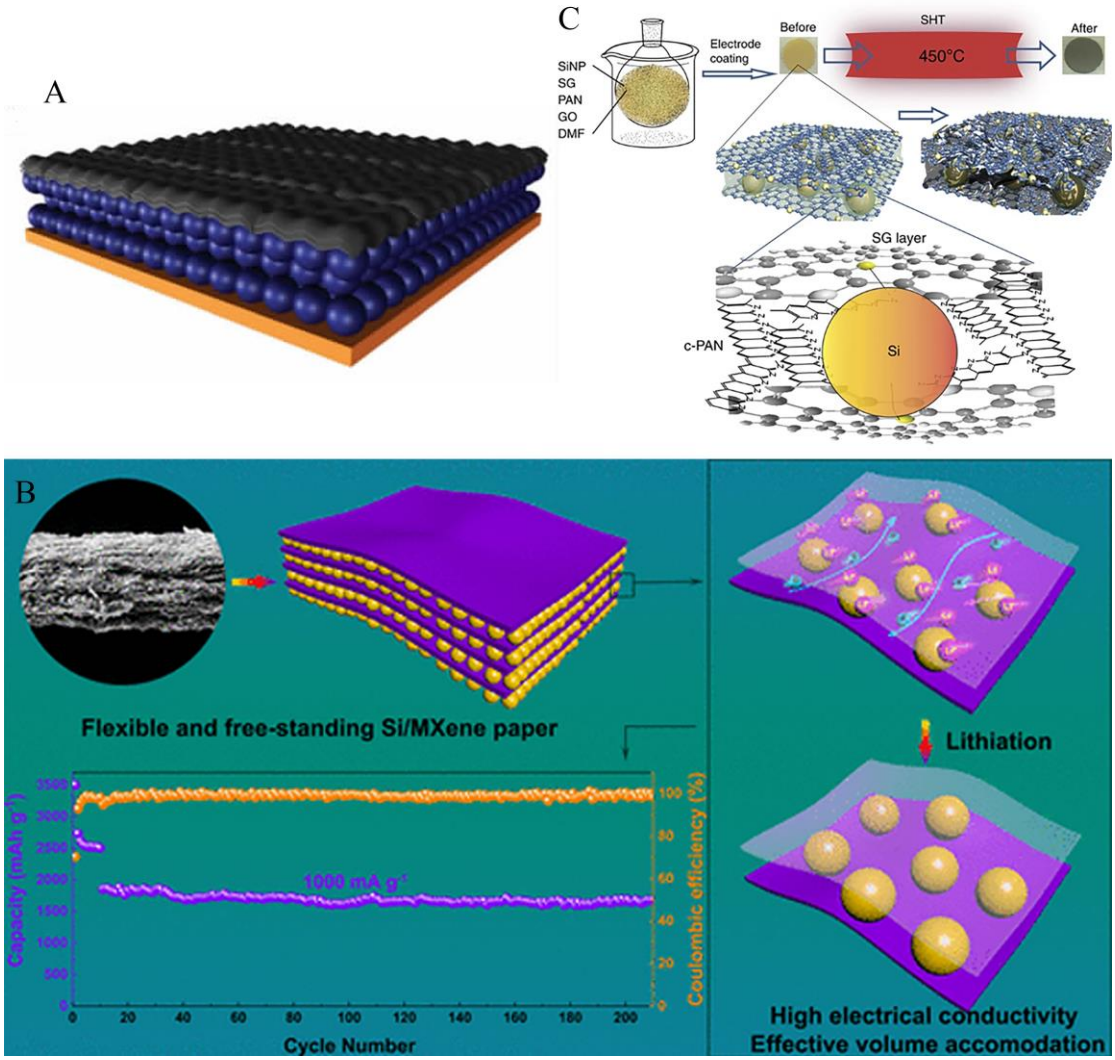


**Figure 6.** A. Schematic diagram of sandwich silicon anode structure. Reproduced with permission.[76] Copyright 2016, Nanoscale. B. Simulation diagram and cycle curve of Si/MXene composite paper. Reproduced with permission.[78] Copyright 2019, American Chemical Society. C. Schematic of the preparation process and structure of the SG. Reproduced with permission.[80] Copyright 2015, Nat Commun.

Similar sandwich structure silicon anodes have been widely noted and studied. Huang et al. [81] prepared graphene/carbon nanotubes/silicon (G/CNT/Si) sandwich structure anodes without binder. Zhang et al. [82] prepared parallelly oriented graphene-sandwiched layered silicon/graphene hybrid microparticles. Huang et al. [83] used in situ polymerized electron conducting PAni hydrogel to connect SiNPs and graphene sheets to prepare the three-dimensional sandwich structure of Si/Polyaniline/Graphene (Figure 7A). This sandwich structure has high conductivity and elasticity, which can accommodate the large volume expansion of silicon. After 50 cycles, the structure of the Si/Polyaniline/Graphene did not rupture. The Si/Polyaniline/Graphene showed a discharge specific capacity of 2708 mAh $g^{-1}$ in the first cycle at 160 mA $g^{-1}$. After several cycles, the specific capacity stabilized at around 1400 mAh $g^{-1}$. There is no significant decrease in capacity after even 250 cycles.

Wei et al. [84] prepared a sandwiched silicon anode that protects silicon under carbon nanotubes. Liu et al. [85] designed a Si/Reduced Graphite Oxide (rGO) bilayer nano sandwich structure (Figure 7B). The characteristic of this structure is that the sandwich structure curls into a multi-layer structure. The gaps within the structure can accommodate volume expansion, and the close combination of rGO and Si increases the conductivity of electrons while preventing excessive SEI caused by direct contact between Si and electrolyte. At a current density of 3 A $g^{-1}$, the discharge specific capacity of

Preprints (www.preprints.org) | NOT PEER-REVIEWED | Posted: 5 July 2023 doi:10.20944/preprints202307.0292.v1



the first cycle is 1642 mAh $g^{-1}$. After 2000 cycles, it is found that the specific capacity loss rate for every 100 cycles is only 3.3%.

Huang et al. [86] prepared a symmetrical sandwich structure SiN/Si/SiN composite anode with good cycling performance. Jia et al. [87] used self-assembly technology to prepare biomimetic sandwich structure carbon/silicon/titanium oxide nanofiber composites. Zhang et al. [88] prepared a carbon/silicon/hematite multilayer electrode by simple mixing and heat treatment (Figure 7C). Dissolving $FeCl_3 \cdot 6H_2O$ in oleic acid and undergoing simple treatment, carbon sheets with iron oxide embeddings can be obtained. Finally, silicon is mixed and annealed to obtain electrodes with silicon sandwiched between the carbon sheets. Iron oxide expands in addition to silicon in this multi-layer electrode, but the space between the carbon layers can accommodate huge volume expansion. At the same time, the carbon layer also improves the flexibility and conductivity of the electrode. At a current density of 750 mA $g^{-1}$, a high specific capacity of 1980 mAh $g^{-1}$ could be obtained after 250 cycles.

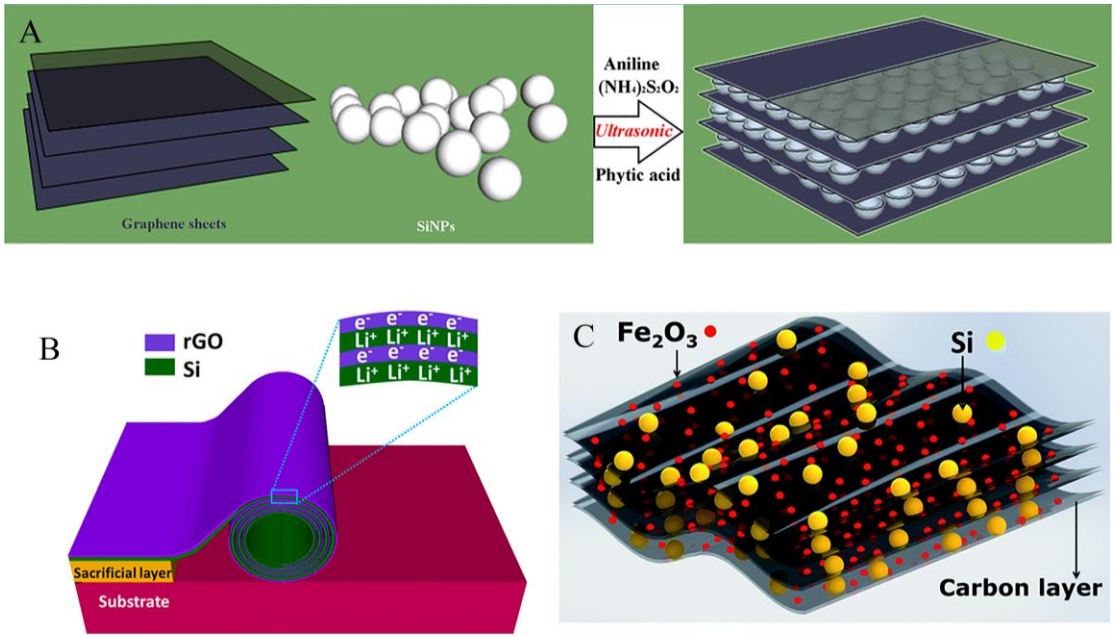


**Figure 7.** A. Fabrication process for 3D Sandwich-like Si/Polyaniline/Graphene nano architecture. Reproduced with permission.[83] Copyright 2018, Ceramics International. B. Schematic fabrication process of the rolled-up Si/rGO bilayer nanomembranes. Reproduced with permission.[85] Copyright 2015, *ACS Nano. C.* Schematic of the prepared C-Si-$Fe_2O_3$ composite. Reproduced with permission.[88] Copyright 2016, Journal of Materials Chemistry.

## 5. Artificial SEI

The severe capacity degradation of silicon anode lithium-ion batteries is not only due to the expansion and pulverization of silicon particles, but also partly due to the rupture and regeneration of SEI caused by volume expansion, which continuously consumes lithium ions. The continuous thickening of SEI is also not conducive to ion transport. SEI can transport lithium ions while isolating electrons. An ideal SEI should have high ion transport capability and low electron transport capability. Artificial SEI, also known as an artificial solid electrolyte, prevents direct contact between silicon particles and electrolyte. Some artificial SEI can provide a portion of lithium ions during the first cycle, improving the initial Coulombic efficiency of batteries. It can also reduce the capture of lithium in long-term cycles, improving the capacity retention rate and Coulombic efficiency of lithium-ion batteries. Moreover, artificial SEI can also provide stress to confront and buffer the expansion of silicon anodes.

Chen et al. [89] prepared S-containing artificial SEI by nucleophilic reaction of sulfide and ester-based electrolyte. Li et al. [90] used solid electrolyte material lithium nitride phosphorus oxide

 doi:10.20944/preprints202307.0292.v1



(Lipon) to prepare artificial SEI to solve the problem of electrochemical performance degradation. Lipon can transport ions and isolate electrons. Research has found that the critical thickness of the SEI prepared by Lipon is 40-50 nm. When the thickness does not exceed 50 nm, the capacity does not significantly decrease after 100 cycles. When the thickness is greater than 50 nm, the reversible capacity decreases due to the additional ion resistance provided by the excessively thick SEI. However, when the thickness is 20 nm, the prevention of charge loss is limited, and the Coulombic efficiency is about 98%. On the contrary, when the thickness exceeds 50 nm, the effect of preventing electrolyte decomposition is significant, and the Coulombic efficiency increases to over 99%. Lipon's SEI isolates electrons, preventing electrolyte from continuously decomposing in the SEI, suppressing capacity loss, and improving Coulombic efficiency.

In the study of Wang et al. [91], N-containing functional groups form a uniform and thin layer on the surface after strong interaction with Si particles, and decompose to form N-rich inorganic solid electrolyte interface (SEI) layer. Bolloju et al. [92] reported a novel artificial SEI by adding polymer artificial SEI (A-SEI) to the porous structure of Si/GR composites (Figure 8A). The A-SEI through a simple and scalable early wetting impregnation (IWI) method, formed by in-situ polymerization of SCS and GA. This preparation method induces more porosity, prevents the electrolyte from entering the porous structure, and prevents direct contact between Si and the electrolyte. Adding A-SEI improves cycle stability, and batteries containing 3 wt% polymers perform best. After 300 cycles, the capacity retention rate was 74.1%.

To inhibit the reaction of solid electrolytes, Ronneburg [93] designed alumina as artificial SEI. Covalent organic frameworks (COFs) are widely used due to their high porosity and controllable shape. Ai et al. [94] synthesized COF artificial SEI on the surface of Si particles using a two-step method (Figure 8B). The SEI coating of COF effectively reduces the decomposition of the electrolyte, resulting in higher Coulombic efficiency and cycling stability of Si electrodes, as well as improving rate performance. Meanwhile, the SEI coating of COF improves ion transfer efficiency. At a high current density of 2 A $g^{-1}$, the COF-coated electrode showed a reversible specific capacity of 1864 mAh $g^{-1}$ and a cycling retention rate of 60% after 1000 cycles.

Cao et al. [95] designed a multifunctional artificial solid electrolyte, which was processed and finally self-polymerized to obtain poly-4-trifluoromethylphenylboronic acid (PTFPBA) with repeated B−O chains. Zhou et al. [96] directly constructed a multifunctional polypyrrole protective layer on the surface of silicon nanoparticles as artificial SEI. Chen et al. [97] constructed a multi-component puzzle-shaped artificial SEI by combining fluoro silane and polyether silane (Figure 8C). The application of fluorinated groups produces a uniform and dense structure for the electrode, ethylene glycol as the main chain promotes ion transport efficiency. The multi-component spliced network improves the mechanical properties of the SEI structure. This SEI structure allows the electrode to maintain stable lithium removal and insertion for up to 500 h in a corrosive carbonate-based electrolyte.

Jin et al. [98] designed a self-repairing artificial SEI (aSEI) that includes Si in $TiO_2$ shells and thin carbon shells (Figure 8D), with pores between the two, which can accommodate the expansion of silicon particles and inject electrolyte. Initially, $TiO_2$ may not be completely sealed, leading to the electrolyte influx. However, during the first cycle, the expansion of silicon will squeeze out the electrolyte, and the contact between the electrolyte and silicon will generate natural SEI (nSEI), which will automatically repair aSEI. At 0.5 C, the specific capacity exceeds 990 mAh $g^{-1}$, and the Coulombic efficiency is above 99.9% after 1500 cycles.

Harpak et al. [99] deposited the parylene layer as an artificial elastic SEI layer for three-dimensional nano silicon anodes. Mu et al. [100] prepared artificial SEI through molecular layer deposition (MLD), depositing a conformal polyurea layer with hydrogen bonds and polar functional groups on a silicon electrode (Figure 8E). This organic coating improves the ion diffusion rate, which is conducive to forming stable SEI. At the same time, the mechanical properties of the interface buffer the expansion of silicon volume, ensuring the integrity of the electrode. The electrode with added coating has good cycling stability and rate performance, with a specific capacity of 1010 mAh $g^{-1}$ at a current density of 800 mA $g^{-1}$ after 1000 cycles.

Preprints (www.preprints.org) | NOT PEER-REVIEWED | Posted: 5 July 2023 doi:10.20944/preprints202307.0292.v1



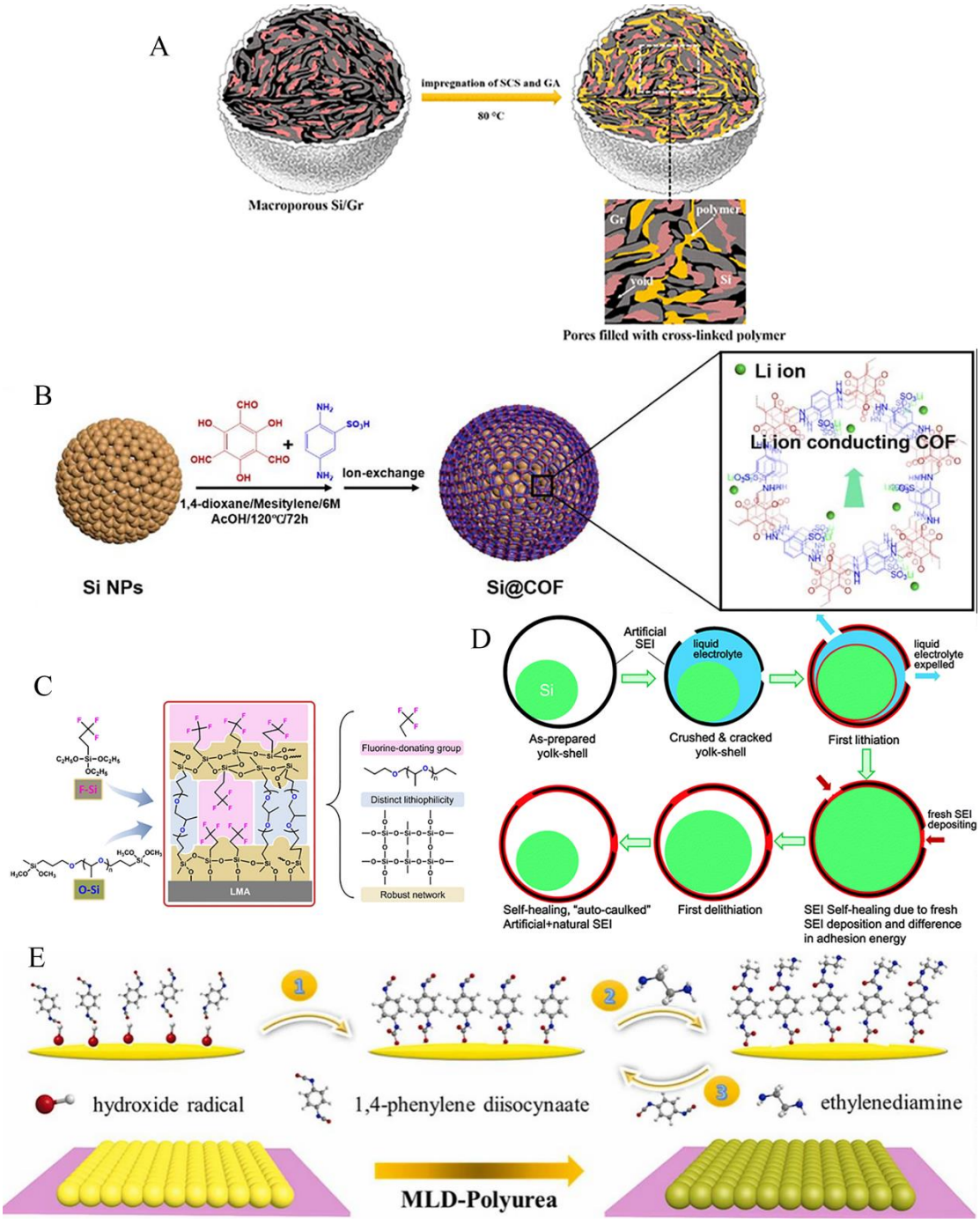


**Figure 8.** A. Schematic diagram of in-situ crosslinking polymer coating on Si/Gr composite particles using the IWI method. Reproduced with permission.[92] Copyright 2023, American Chemical Society. B. Schematic illustration of preparation of Si@COF NPs. Reproduced with permission.[94] Copyright 2020, Nano Energy. C. Schematic illustration of designing multi-component jigsaw-like artificial SEI, where the fluorine-donating group (i.e., $-CF_3$) could yield a dense structure to prevent the formation of Li dendrites and the decomposition of electrolytes, the ethylene glycol backbone is favorable for rapid $Li^+$ transport, the robust cross-linking network could endow the SEI layer with excellent mechanical strength. Reproduced with permission.[97] Copyright 2023, Commun Mater. D. Schematic illustrations of self-healing in a yolk-shell SiMA. Reproduced with permission.[98] Copyright 2017, Energy & environmental science. E. The preparation process diagram of the MLD-polyurea coated silicon electrode. Reproduced with permission.[100] Copyright 2022, Nano Energy.

## 6. Summary and Outlook

In response to the problem caused by excessive volume expansion of silicon anode, this article summarizes the research on the structural design and optimization of silicon anode from the aspects of reducing the dimension of silicon particles, optimizing the surface structure of silicon anode, and artificial SEI.

Silicon particles with smaller sizes have a larger specific surface area and smaller expansion stress, resulting in a smaller volume expansion effect. Many studies have prepared silicon into various nanoscale structures, and the results have shown that nanoscale silicon particles have smaller expansion and lower degrees of pulverization. Nanosized particles shorten the ion migration distance and improve reaction efficiency, so it has higher cycling stability and specific capacity.

There are two primary purposes for optimizing silicon particles from the surface. On the one hand, it provides a buffering effect for the expansion of silicon particles. On the other hand, it prevents direct contact between silicon particles and electrolyte. Most silicon anode surface optimizations are achieved through various forms of carbon, and carbon can also improve the poor conductivity of silicon particles.

Unlike graphite anodes, silicon anodes cannot form a passive SEI, and volume expansion leads to the rupture of SEI. Si contacting with electrolyte will continuously regenerate SEI and consume some lithium ions, leading to severe capacity fade and a decrease in Coulombic efficiency. The addition of artificial SEI could solve these problems by preventing Si from contact with electrolyte, which reduces electrolyte consumption, and improves specific capacity and cycling performance.

Except for addressing the issues caused by volume expansion and poor conductivity of silicon anode, achieving commercialization requires a simple and low-cost preparation technology. Preparing nano silicon particles or nanocomposite structures is insufficient to achieve this goal. In future research, while improving electrochemical performance, simple and scalable methods should be explored to achieve the commercialization goal of silicon anode.

**Declaration of competing interest:** The authors declare that they have no known competing financial interests or personal relationships that could have appeared to influence the work reported in this paper.

**Acknowledgments:** This work was funded by the Thousand Talents Plan Project of Jiangxi Province (jxsq2020101053 to Guoxing Qu). The authors would like to acknowledge the support from the open fund of the key laboratory of advanced energy materials chemistry of Nankai University.

## References

1. Goodenough, J.B.; Kim, Y. Challenges for rechargeable Li batteries. *Chem. Mater.* **2010**, 22, 587-603.
2. Dunn, B.; Kamath, H.; Tarascon, J.-M. Electrical energy storage for the grid: a battery of choices. *Science*. **2011**, 334, 928-935.
3. Brandt, K. Historical development of secondary lithium batteries. *Solid State Ionics*. **1994**, 69, 173-183.
4. Jeong, G.; Kim, Y.-U.; Kim, H.; Kim, Y.-J.; Sohn, H.-J. Prospective materials and applications for Li secondary batteries. *Energy Environ. Sci.* **2011**, 4, 1986.
5. Tarascon, J.M.; Armand, M. Issues and challenges facing rechargeable lithium batteries. *Nature*. **2001**, 414, 359-367.
6. Bruce, P.G.; Scrosati, B.; Tarascon, J.-M. Nanomaterials for rechargeable lithium batteries. *Angew. Chem. Int. Ed.* **2008**, 47, 2930-2946.
7. Aricò, A.S.; Bruce, P.; Scrosati, B.; Tarascon, J.-M.; van Schalkwijk, W. Nanostructured materials for advanced energy conversion and storage devices. *Nat. Mater.* **2005**, 4, 366-377.
8. Abraham, K.M. Prospects and Limits of energy storage in batteries. *The Journal of Physical Chemistry Letters*. **2015**, 6, 830-844.
9. Ding, N.; Xu, J.; Yao, Y.; Wegner, G.; Lieberwirth, I.; Chen, C. Improvement of cyclability of Si as anode for Li-ion batteries. *J. Power Sources*. **2009**, 192, 644-651.
10. Goriparti, S.; Miele, E.; De Angelis, F.; Di Fabrizio, E.; Proietti Zaccaria, R.; Capiglia, C. Review on recent progress of nanostructured anode materials for Li-ion batteries. *J. Power Sources*. **2014**, 257, 421-443.
11. Du, F.-H.; Wang, K.-X.; Chen, J.-S. Strategies to succeed in improving the lithium-ion storage properties of silicon nanomaterials. *J. Mater. Chem. A*. **2016**, 4, 32-50.
12. Feng, K.; Li, M.; Liu, W.; Kashkooli, A.G.; Xiao, X.; Cai, M.; Chen, Z. Silicon-based anodes for lithium-ion batteries: From fundamentals to practical applications. *Small*. **2018**, 14, 1702737.

13. Sun, Y.; Liu, N.; Cui, Y. Promises and challenges of nanomaterials for lithium-based rechargeable batteries. *Nature Energy*. **2016**, 1, 16071.
14. Wu, H.; Zheng, G.; Liu, N.; Carney, T.J.; Yang, Y.; Cui, Y. Engineering empty space between Si nanoparticles for lithium-ion battery anodes. *Nano Lett.* **2012**, 12, 904-909.
15. Demirkan, M.T.; Yurukcu, M.; Dursun, B.; Demir-Cakan, R.; Karabacak, T. Evaluation of double-layer density modulated Si thin films as Li-ion battery anodes. *Materials Research Express*. **2017**, 4.
16. Lee, K.S.; Lee, S.H.; Woo, S.P.; Kim, H.S.; Yoon, Y.S. Fabrication of amorphous Si and C anode films via co-sputtering for an all-solid-state battery. *Thin Solid Films*. **2014**, 564, 58-64.
17. Chen, Z.H.; Jia, H.; Hoeppener, S.; Friebe, C.; Wang, J.D.; Chanteux, G.; Xie, D.J.; Lu, Y.; Vlad, A.; Schubert, U.S.; Gohy, J.F. Hollow porous silicon nanospheres with 3D SiC@C coating as high-performance anodes. *Mater. Design.* **2023**, 226.
18. Park, M.S.; Park, E.; Lee, J.; Jeong, G.; Kim, K.J.; Kim, J.H.; Kim, Y.J.; Kim, H. Hydrogen silsequioxane-derived Si/SiOx nanospheres for high-capacity lithium storage materials. *ACS Appl. Mater. Interfaces*. **2014**, 6, 9608-9613.
19. Nugroho, A.P.; Hawari, N.H.; Prakoso, B. Vertically aligned n-type silicon nanowire array as a free-standing anode for lithium-ion batteries. **2021**, 11.
20. Zhao, Y.; Peng, L.L.; Ding, Y.; Yu, G.H. Amorphous silicon honeycombs as a binder/carbon-free, thin-film Li-ion battery anode. *Chem. Commun.* **2014**, 50, 12959-12962.
21. Bang, B.M.; Kim, H.; Lee, J.P.; Cho, J.; Park, S. Mass production of uniform-sized nanoporous silicon nanowire anodes via block copolymer lithography. *Energy Environ. Sci.* **2011**, 4, 3395-3399.
22. Chan, C.K.; Peng, H.; Liu, G.; McIlwrath, K.; Zhang, X.F.; Huggins, R.A.; Cui, Y. High-performance lithium battery anodes using silicon nanowires. *Nat. Nanotechnol.* **2008**, 3, 31-35.
23. Tamirat, A.G.; Lui, Y.; Dong, X.; Wang, C.; Wang, Y.; Xia, Y. Ultrathin silicon nanolayer implanted NixSi/Ni nanoparticles as superlong-cycle lithium-ion anode material. *Small Structures*. **2021**, 2, 2000126.
24. Sakabe, J.; Ohta, N.; Ohnishi, T.; Mitsuishi, K.; Takada, K. Porous amorphous silicon film anodes for high-capacity and stable all-solid-state lithium batteries. *Communications Chemistry*. **2018**, 1, 24.
25. Wang, M.X.; Geng, Z.R. Facile synthesis of multilayer-like Si thin film as high-performance anode materials for lithium-ion batteries. *Appl. Phys. A-mater.* **2016**, 122.
26. Chen, L.B.; Xie, J.Y.; Yu, H.C.; Wang, T.H. An amorphous Si thin film anode with high capacity and long cycling life for lithium ion batteries. *J. Appl. Electrochem.* **2009**, 39, 1157-1162.
27. Sung, J.; Kim, N.; Ma, J.; Lee, J.H.; Joo, S.H.; Lee, T.; Chae, S.; Yoon, M.; Lee, Y.; Hwang, J.; Kwak, S.K.; Cho, J. Subnano-sized silicon anode via crystal growth inhibition mechanism and its application in a prototype battery pack. *Nature Energy*. **2021**, 6, 1164-1175.
28. Karuppiah, S.; Keller, C.; Kumar, P.; Jouneau, P.-H.; Aldakov, D.; Ducros, J.-B.; Lapertot, G.; Chenevier, P.; Haon, C. A Scalable silicon nanowires-grown-on-graphite composite for high-energy lithium batteries. *ACS Nano*. **2020**, 14, 12006-12015.
29. Wen, Z.H.; Lu, G.H.; Mao, S.; Kim, H.; Cui, S.M.; Yu, K.H.; Huang, X.K.; Hurley, P.T.; Mao, O.; Chen, J.H. Silicon nanotube anode for lithium-ion batteries. *Electrochem. Commun.* **2013**, 29, 67-70.
30. Park, M.-H.; Kim, M.G.; Joo, J.; Kim, K.; Kim, J.; Ahn, S.; Cui, Y.; Cho, J. Silicon nanotube battery anodes. *Nano Lett.* **2009**, 9, 3844-3847.
31. Ashuri, M.; He, Q.R.; Liu, Y.Z.; Zhang, K.; Emani, S.; Sawicki, M.S.; Shamie, J.S.; Shaw, L.L. Hollow silicon nanospheres encapsulated with a thin carbon shell: an electrochemical study. *Electrochim. Acta*. **2016**, 215, 126-141.
32. Liang, J.W.; Li, X.N.; Zhu, Y.C.; Guo, C.; Qian, Y.T. Hydrothermal synthesis of nano-silicon from a silica sol and its use in lithium ion batteries. *Nano Research*. **2015**, 8, 1497-1504.
33. Pu, J.; Qin, J.; Wang, Y.; Qiao, Z.; Yu, X.; Xu, J.; Zhang, X.Ruan, D. Synthesis of micro-nano sphere structure silicon–carbon composite as anode material for lithium-ion batteries. *Chemical Physics Letters*. **2022**, 806, 140006.
34. Tesfaye, A.T.; Gonzalez, R.; Coffer, J.L.; Djenizian, T. Porous silicon nanotube arrays as anode material for Li-Ion batteries. *ACS Appl. Mater. Interfaces*. **2015**, 7, 20495-20498.
35. Saager, S.; Scheffel, B.; Zywitzki, O.; Modes, T.; Piwko, M.; Doerfler, S.; Althues, H.; Metzner, C. Porous silicon thin films as anodes for lithium ion batteries deposited by co-evaporation of silicon and zinc. *Surface and Coatings Technology*. **2019**, 358, 586-593.
36. Kim, Y.M.; Ahn, J.; Yu, S.H.; Chung, D.Y.; Lee, K.J.; Lee, J.K.; Sung, Y.E. Titanium silicide coated porous silicon nanospheres as anode materials for lithium ion batteries. *Electrochim. Acta*. **2015**, 151, 256-262.
37. Li, X.; Gu, M.; Hu, S.; Kennard, R.; Yan, P.; Chen, X.; Wang, C.; Sailor, M.J.; Zhang, J.-G.; Liu, J. Mesoporous silicon sponge as an anti-pulverization structure for high-performance lithium-ion battery anodes. *Nat. Commun.* **2014**, 5, 4105.
38. Yan, Z.; Jiang, J.; Zhang, Y.; Yang, D.; Du, N. Scalable and low-cost synthesis of porous silicon nanoparticles as high-performance lithium-ion battery anode. *Materials Today Nano*. **2022**, 18.

39. Ge, M.Y.; Rong, J.P.; Fang, X.; Zhou, C.W. Porous doped silicon nanowires for lithium ion battery anode with long cycle life. *Nano Lett.* **2012**, 12, 2318-2323.
40. Xiao, Q.; Gu, M.; Yang, H.; Li, B.; Zhang, C.; Liu, Y.; Liu, F.; Dai, F.; Yang, L.; Liu, Z.; Xiao, X.; Liu, G.; Zhao, P.; Zhang, S.; Wang, C.; Lu, Y.; Cai, M. Inward lithium-ion breathing of hierarchically porous silicon anodes. *Nat. Commun.* **2015**, 6, 8844.
41. An, W.; Gao, B.; Mei, S.; Xiang, B.; Fu, J.; Wang, L.; Zhang, Q.; Chu, P.K.; Huo, K. Scalable synthesis of ant-nest-like bulk porous silicon for high-performance lithium-ion battery anodes. *Nat. Commun.* **2019**, 10, 1447.
42. Dong, H.; Fu, X.L.; Wang, J.; Wang, P.; Ding, H.; Song, R.; Wang, S.M.; Li, R.R.; Li, S.Y. In-situ construction of porous Si@C composites with LiCl template to provide silicon anode expansion buffer. *Carbon*. **2021**, 173, 687-695.
43. Hu, Y.S.; Adelhelm, P.; Smarsly, B.M.; Maier, J. Highly stable lithium storage performance in a porous carbon/silicon nanocomposite. *Chemsuschem*. **2010**, 3, 231-235.
44. Jia, H.; Li, X.; Song, J.; Zhang, X.; Luo, L.; He, Y.; Li, B.; Cai, Y.; Hu, S.; Xiao, X.; Wang, C.; Rosso, K.M.; Yi, R.; Patel, R.; Zhang, J.-G. Hierarchical porous silicon structures with extraordinary mechanical strength as high-performance lithium-ion battery anodes. *Nat. Commun.* **2020**, 11, 1474.
45. Guo, J.C.; Chen, X.L.; Wang, C.S. Carbon scaffold structured silicon anodes for lithium-ion batteries. *J. Mater. Chem.* **2010**, 20, 5035-5040.
46. Dong, Z.; Du, W.; Gu, H.; Long, Y.; Zhang, C.; Chen, G.; Feng, Z.; Sun, W.; Jiang, Y.; Liu, Y.; Yang, Y.; Gan, J.; Gao, M.; Pan, H. A unique structural highly compacted binder-free silicon-based anode with high electronic conductivity for high-performance lithium-ion batteries. *Small Structures*. **2022**, 3, 2100174.
47. Favors, Z.; Bay, H.H.; Mutlu, Z.; Ahmed, K.; Ionescu, R.; Ye, R.; Ozkan, M.; Ozkan, C.S. Towards scalable binderless electrodes: carbon coated silicon nanofiber paper via Mg reduction of electrospun $SiO_2$ nanofibers. *Sci. Rep.* **2015**, 5, 8246.
48. Zhu, R.Y.; Wang, Z.H.; Hu, X.J.; Liu, X.J.; Wang, H. Silicon in hollow carbon nanospheres assembled microspheres cross-linked with N-doped carbon fibers toward a binder free, high performance, and flexible anode for lithium-ion batteries. *Adv. Funct. Mater.* **2021**, 31.
49. Zhang, W.; Zuo, P.J.; Chen, C.; Ma, Y.L.; Cheng, X.Q.; Du, C.Y.; Gao, Y.Z.; Yin, G.P. Facile synthesis of binder-free reduced graphene oxide/silicon anode for high-performance lithium ion batteries. *J. Power Sources*. **2016**, 312, 216-222.
50. Liu, B.; Wang, X.; Chen, H.; Wang, Z.; Chen, D.; Cheng, Y.B.; Zhou, C.; Shen, G. Hierarchical silicon nanowires-carbon textiles matrix as a binder-free anode for high-performance advanced lithium-ion batteries. *Sci. Rep.* **2013**, 3, 1622.
51. Wang, W.; Epur, R.; Kumta, P.N. Vertically aligned silicon/carbon nanotube (VASCNT) arrays: Hierarchical anodes for lithium-ion battery. *Electrochem. Commun.* **2011**, 13, 429-432.
52. Haro, M.; Kumar, P.; Zhao, J.; Koutsogiannis, P.; Porkovich, A.J.; Ziadi, Z.; Bouloumis, T.; Singh, V.; Juarez-Perez, E.J.; Toulkeridou, E.; Nordlund, K.; Djurabekova, F.; Sowwan, M.; Grammatikopoulos, P. Nano-vault architecture mitigates stress in silicon-based anodes for lithium-ion batteries. *Communications Materials*. **2021**, 2, 16.
53. Wang, B.; Li, X.L.; Zhang, X.F.; Luo, B.; Jin, M.H.; Liang, M.H.; Dayeh, S.A.; Picraux, S.T.; Zhi, L.J. Adaptable silicon-carbon nanocables sandwiched between reduced graphene oxide sheets as lithium ion battery anodes. *ACS Nano*. **2013**, 7, 1437-1445.
54. Li, Y.; Xu, G.; Yao, Y.; Xue, L.; Yanilmaz, M.; Lee, H.; Zhang, X. Coaxial electrospun Si/C–C core–shell composite nanofibers as binder-free anodes for lithium-ion batteries. *Solid State Ionics*. **2014**, 258, 67-73.
55. Shao, F.; Li, H.; Yao, L.; Xu, S.W.; Li, G.; Li, B.; Zou, C.; Yang, Z.; Su, Y.J.; Hu, N.T.; Zhang, Y.F. Binder-free, flexible, and self-standing non-woven fabric anodes based on graphene/Si hybrid fibers for high-performance Li-ion batteries. *ACS Appl. Mater. Interfaces*. **2021**, 13, 27270-27277.
56. Liu, Q.; Gao, Y.; He, P.; Yan, C.; Gao, Y.; Gao, J.; Lu, H.; Yang, Z. Facile fabrication of hollow structured Si-Ni-C nanofabric anode for Li-ion battery. *Materials Letters*. **2018**, 231, 205-208.
57. Osaka, T.; Nara, H.; Momma, T.; Yokoshima, T. New Si-O-C composite film anode materials for LIB by electrodeposition. *J. Mater. Chem. A*. **2014**, 2, 883-896.
58. Yang, Y.; Chen, D.; Liu, B.; Zhao, J. Binder-free Si nanoparticle electrode with 3D porous structure prepared by electrophoretic deposition for lithium-ion batteries. *ACS Appl. Mater. Interfaces*. **2015**, 7, 7497-7504.
59. Song, S.G.; Li, J.C.; Zheng, A.Q.; Yang, Y.Q.; Yin, K.B. Facile synthesis of sponge-like porous nano carbon-coated silicon anode with tunable pore structure for high-stability lithium-ion batteries. *Molecules*. **2021**, 26.
60. Tan, W.; Yang, F.; Lu, Z.G.; Xu, Z.H. A design strategy of carbon coatings on silicon nanoparticles as anodes of high-performance lithium-ion batteries. *ACS Applied Energy Materials*. **2022**, 5, 12143-12150.
61. Guan, P.; Li, J.; Lu, T.; Guan, T.; Ma, Z.; Peng, Z.; Zhu, X.; Zhang, L. Facile and scalable approach to fabricate granadilla-like porous-structured silicon-based anode for lithium ion batteries. *ACS Appl. Mater. Interfaces*. **2018**, 10, 34283-34290.

62. Ma, X.; Hou, G.; Ai, Q.; Zhang, L.; Si, P.; Feng, J.; Ci, L. A heart-coronary arteries structure of carbon nanofibers/graphene/silicon composite anode for high performance lithium ion batteries. *Sci. Rep.* **2017**, 7, 9642.
63. Li, Q.L.; Chen, D.Q.; Li, K.; Wang, J.; Zhao, J.B. Electrostatic self-assembly bmSi@C/rGO composite as anode material for lithium ion battery. *Electrochim. Acta*. **2016**, 202, 140-146.
64. Feng, Y.; Zhang, Y.; Song, Y.; Li, P.; Liu, J. Binary carbon modification promoting the electrochemical performance of silicon anode for lithium-ion batteries. *ChemistrySelect*. **2023**, 8, e202204086.
65. Chen, H.X.; Xiao, Y.; Wang, L.; Yang, Y. Silicon nanowires coated with copper layer as anode materials for lithium-ion batteries. *J. Power Sources*. **2011**, 196, 6657-6662.
66. Baek, S.H.; Park, J.S.; Jeong, Y.M.; Kim, J.H. Facile synthesis of Ag-coated silicon nanowires as anode materials for high-performance rechargeable lithium battery. *J. Alloy. Compd.* **2016**, 660, 387-391.
67. Chan, C.K.; Patel, R.N.; O'Connell, M.J.; Korgel, B.A.; Cui, Y. Solution-grown silicon nanowires for lithium-ion battery anodes. *ACS Nano*. **2010**, 4, 1443-1450.
68. Wu, C.-Y.; Chang, C.-C.; Duh, J.-G. Silicon nitride coated silicon thin film on three dimensions current collector for lithium ion battery anode. *J. Power Sources*. **2016**, 325, 64-70.
69. He, Y.; Yu, X.Q.; Wang, Y.H.; Li, H.; Huang, X.J. Alumina-coated patterned amorphous silicon as the anode for a lithium-ion battery with high coulombic efficiency. *Adv. Mater.* **2011**, 23, 4938-4941.
70. Zhang, Z.; Xi, F.S.; Chen, X.H.; Li, S.Y.; Ma, W.H.; Ding, Z.; Qu, T.; Dai, Y.N.; Deng, R. Improved lithium-ion batteries with coral-like anodes made of recycled spherical porous silicon coated with nitrogen-doped carbon. *Environmental Chemistry Letters*. **2022**, 20, 3377-3385.
71. Kong, X.; Zheng, Y.; Wang, Y.; Liang, S.; Cao, G.; Pan, A. Necklace-like Si@C nanofibers as robust anode materials for high performance lithium ion batteries. *Science Bulletin*. **2019**, 64, 261-269.
72. Song, J.X.; Chen, S.R.; Zhou, M.J.; Xu, T.; Lv, D.P.; Gordin, M.L.; Long, T.J.; Melnyk, M.; Wang, D.H. Micro-sized silicon-carbon composites composed of carbon-coated sub-10 nm Si primary particles as high-performance anode materials for lithium-ion batteries. *J. Mater. Chem. A*. **2014**, 2, 1257-1262.
73. Li, B.; Yao, F.; Bae, J.J.; Chang, J.; Zamfir, M.R.; Le, D.T.; Pham, D.T.; Yue, H.; Lee, Y.H. Hollow carbon nanospheres/silicon/alumina core-shell film as an anode for lithium-ion batteries. *Sci. Rep.* **2015**, 5, 7659.
74. Wu, H.; Yu, G.; Pan, L.; Liu, N.; McDowell, M.T.; Bao, Z.; Cui, Y. Stable Li-ion battery anodes by in-situ polymerization of conducting hydrogel to conformally coat silicon nanoparticles. *Nat. Commun.* **2013**, 4, 1943.
75. Xu, Y.H.; Yin, G.P.; Cheng, X.Q.; Zuo, P.J. Enhanced lithium storage performance of silicon anode via fabricating into sandwich electrode. *Electrochim. Acta*. **2011**, 56, 4403-4407.
76. Zhao, C.; Luo, X.; Chen, C.; Wu, H. Sandwich electrode designed for high performance lithium-ion battery. *Nanoscale*. **2016**, 8, 9511-9516.
77. Zhang, F.; Jia, Z.R.; Wang, C.; Feng, A.L.; Wang, K.K.; Hou, T.Q.; Liu, J.J.; Zhang, Y.; Wu, G.L. Sandwich-like silicon/$Ti_3C_2Tx$ MXene composite by electrostatic self-assembly for high performance lithium ion battery. *Energy*. **2020**, 195.
78. Tian, Y.; An, Y.; Feng, J. Flexible and freestanding silicon/MXene composite papers for high-performance lithium-ion batteries. *ACS Appl. Mater. Interfaces*. **2019**, 11, 10004-10011.
79. Sun, Z.X.; Wang, G.J.; Cai, T.W.; Ying, H.J.; Han, W.Q. Sandwich-structured graphite-metallic silicon@C nanocomposites for Li-ion batteries. *Electrochim. Acta*. **2016**, 191, 299-306.
80. Hassan, F.M.; Batmaz, R.; Li, J.; Wang, X.; Xiao, X.; Yu, A.; Chen, Z. Evidence of covalent synergy in silicon–sulfur–graphene yielding highly efficient and long-life lithium-ion batteries. *Nat. Commun.* **2015**, 6, 8597.
81. Huang, Z.D.; Zhang, K.; Zhang, T.T.; Liu, R.Q.; Lin, X.J.; Li, Y.; Feng, X.M.; Mei, Q.B.; Masese, T.; Ma, Y.W.; Huang, W. Binder-free graphene/carbon nanotube/silicon hybrid grid as freestanding anode for high capacity lithium ion batteries. *Compos. Part. A-appl. S.* **2016**, 84, 386-392.
82. Zhang, X.H.; Wang, D.H.; Zhang, S.Y.; Li, X.L.; Zhi, L.J. A hierarchical layering design for stable, self-restrained and high volumetric binder-free lithium storage. *Nanoscale*. **2019**, 11, 21728-21732.
83. Huang, R.-a.; Guo, Y.; Chen, Z.; Zhang, X.; Wang, J.; Yang, B. An easy and scalable approach to synthesize three-dimensional sandwich-like Si/Polyaniline/Graphene nanoarchitecture anode for lithium ion batteries. *Ceram. Int.* **2018**, 44, 4282-4286.
84. Wei, D.H.; Gao, X.; Zeng, S.Y.; Li, H.B.; Li, H.Y.; Li, W.Z.; Tao, X.Q.; Xu, L.L.; Chen, P. Improving the performance of micro-silicon anodes in lithium-ion batteries with a functional carbon nanotube interlayer. *Chemelectrochem*. **2018**, 5, 3143-3149.
85. Liu, X.; Zhang, J.; Si, W.; Xi, L.; Eichler, B.; Yan, C.; Schmidt, O.G. Sandwich nanoarchitecture of Si/reduced graphene oxide bilayer nanomembranes for Li-ion batteries with long cycle life. *ACS Nano*. **2015**, 9, 1198-1205.
86. Huang, X.D.; Zhang, F.; Cao, Y.Z.; Huang, Q.A. Symmetrical sandwich-structured SiN/Si/SiN composite for lithium-ion battery anode with improved cyclability and rate capacity. *J. Electrochem. Soc.* **2018**, 165, A3397-A3402.

87. Jia, D.L.; Li, X.; Huang, J.G. Bio-inspired sandwich-structured carbon/silicon/titanium-oxide nanofibers composite as an anode material for lithium-ion batteries. *Compos. Part. A-appl. S*. **2017**, 101, 273-282.
88. Zhang, L.; Guo, H.; Rajagopalan, R.; Hu, X.; Huang, Y.; Dou, S.X.; Liu, H.K. One-step synthesis of a silicon/hematite@carbon hybrid nanosheet/silicon sandwich-like composite as an anode material for Li-ion batteries. *J. Mater. Chem. A*. **2016**, 4, 4056-4061.
89. Chen, W.L.; Chen, K.Y.; Zeng, R.; Wan, M.; Guo, Y.X.; Liao, Y.Q.; Peng, J.Y.; Zhang, W.X.; Huang, Y.H. In situ construction of S-based artificial solid electrolyte interphases layer for stable silicon anode in lithium-ion batteries. *ACS Applied Energy Materials*. **2022**, 5, 14136-14143.
90. Li, J.; Dudney, N.J.; Nanda, J.; Liang, C. Artificial solid electrolyte interphase to address the electrochemical degradation of silicon electrodes. *ACS Appl. Mater. Interfaces*. **2014**, 6, 10083-10088.
91. Wang, Y.; Yang, X.; Yuan, Y.; Wang, Z.; Zhang, H.; Li, X. N-rich solid electrolyte interface constructed in situ via a binder strategy for highly stable silicon anode. *Adv. Funct. Mater.*, n/a, 2301716.
92. Bolloju, S.; Abdollahifar, M.; Parthasarathi, S.-K.; Chen, Y.-C.; Weng, Y.-T.; Chao, C.-Y.; Wu, N.-L. Efficient utilization of macropores as artificial solid–electrolyte interphase channels for high-capacity silicon/graphite anode materials. *ACS Sustainable Chemistry & Engineering*. **2023**, 11, 2623-2633.
93. Ronneburg, A.; Silvi, L.; Cooper, J.; Harbauer, K.; Ballauff, M. Solid electrolyte interphase layer formation during lithiation of single-crystal silicon electrodes with a protective aluminum oxide coating. **2021**, 13, 21241-21249.
94. Ai, Q.; Fang, Q.; Liang, J.; Xu, X.; Zhai, T.; Gao, G.; Guo, H.; Han, G.; Ci, L.; Lou, J. Lithium-conducting covalent-organic-frameworks as artificial solid-electrolyte-interphase on silicon anode for high performance lithium ion batteries. *Nano Energy*. **2020**, 72, 104657.
95. Cao, Z.; Zheng, X.Y.; Wang, Y.; Huang, W.B.; Li, Y.C.; Huang, Y.H.; Zheng, H.H. Tailoring a multifunctional, boron and fluoride-enriched solid-electrolyte interphase precursor towards high-rate and stable-cycling silicon anodes. *Nano Energy*. **2022**, 93.
96. Zhou, C.Y.; Gong, X.Z.; Feng, Y.K.; Lu, J.J.; Fu, Y.L.; Wang, Z.; Liu, J.H. Constructing an artificial boundary to regulate solid electrolyte interface formation and synergistically enhance stability of nano-Si anodes. *J. Colloid Interf. Sci*. **2022**, 619, 158-167.
97. Chen, L.; Lai, J.; Li, Z.; Zou, H.; Yang, J.; Ding, K.; Cai, Y.-P.; Zheng, Q. A jigsaw-structured artificial solid electrolyte interphase for high-voltage lithium metal batteries. *Communications Materials*. **2023**, 4, 18.
98. Jin, Y.; Li, S.; Kushima, A.; Zheng, X.; Sun, Y.; Xie, J.; Sun, J.; Xue, W.; Zhou, G.; Wu, J.; Shi, F.; Zhang, R.; Zhu, Z.; So, K.; Cui, Y.; Li, J. Self-healing SEI enables full-cell cycling of a silicon-majority anode with a coulombic efficiency exceeding 99.9%. *Energy Environ. Sci.* **2017**, 10, 580-592.
99. Harpak, N.; Davidi, G.; Patolsky, F. Breathing parylene-based nanothin artificial SEI for highly-stable long life three-dimensional silicon lithium-ion batteries. *Chem. Eng. J.* **2022**, 429.
100. Mu, T.; Sun, Y.; Wang, C.; Zhao, Y.; Doyle-Davis, K.; Liang, J.; Sui, X.; Li, R.; Du, C.; Zuo, P.; Yin, G.; Sun, X. Long-life silicon anodes by conformal molecular-deposited polyurea interface for lithium ion batteries. *Nano Energy*. **2022**, 103, 107829.